JOURNAL OF CATALYSIS 69, 158–171 (1981)

Decomposition of Ammonia on Rhodium Crystals

ATIS VÁVERE[1] AND ROBERT S. HANSEN

Ames Laboratory, USDOE, Department of Chemistry, Iowa State University, Ames, Iowa 50011

Received October 29, 1979; revised January 12, 1981

The rates of ammonia decomposition of (110), (100), and (111) single-crystal faces of rhodium were measured over the temperature range 580–725 K for ammonia pressures ranging from 1×10^{-3} to 500×10^{-3} Torr and hydrogen and nitrogen pressures varying from 1×10^{-3} to 150×10^{-3} Torr and 1×10^{-3} to 250×10^{-3} Torr, respectively. The decomposition rates were proportional to $P_{NH_3}^{1/2}$ and P_{NH_3} at low and high hydrogen pressure, respectively. The H_2 kinetic order varied from 0 (low P_{H_2}) to -1.0 (high P_{H_2}). The rate was independent of nitrogen pressure. Isotope studies indicated that NH_3 decomposes about 1.5 times faster than ND_3 on the (110) and (111) faces. A large face specificity is evident with the rates on the (110) surface over 10 times as great as those on the (111) surface. LEED, AES, and flash desorption experiments indicated that boron (B) was a significant surface "poison" and that the Rh (110) surface under reaction conditions might contain at most moderate coverages of nitrogen adatoms, but that coverages of other species were very small. The LEED/AES characterizations were done in a different system from that used in the kinetic and thermal desorption experiments. Rate expressions consistent with the observed kinetics are derived from a model involving surface species Rh_2NH, RhH, and RhN, with only the RhN coverage being appreciable under the experimental conditions used. The kinetic data for the Rh (110) face are semiquantitatively fit to these rate expressions via a superposition technique and also to an empirical rate expression which functionally is similar to the mechanism rate equation. A decreasing NH_3 order ($<\frac{1}{2}$) at high P_{NH_3} and low T is attributed to the buildup of surface nitrogen. Kinetic orders and activation energies obtained are generally consistent with most other literature data.

INTRODUCTION

Catalytic reactions of nitrogen-containing compounds have long been of interest, and environmental concerns have given a recent emphasis to reactions associated with NO_x decomposition or reduction. It has been postulated that NH_3 may be an intermediate in the reduction of NO_x on automotive exhaust catalysts (*1*). Although the NH_3 decomposition reaction has received considerable attention in the past (*2*), the kinetics and mechanisms of the reaction have generally only been interpreted in terms of the semiempirical Temkin–Pyzhev theory.

Recent studies of the decomposition reaction on single crystals on W (*3*) and Pt (*4*) have provided accurately determined data and novel interpretations of the results obtained. McAllister and Hansen (*3*) proposed a simple yet unique reaction mechanism which did not involve the desorption of N_2 as the rate-limiting step, contrary to the basic Temkin–Pyzhev premise. In the present work, the decomposition of NH_3 was studied over single-crystal Rh catalysts in an effort to determine the kinetics and possible reaction pathways for the process. Rh is a catalyst of interest in that it is a very active NH_3 decomposition catalyst (*5*) relative to W and Pt (*5, 6*) and according to Schlatter and Taylor (*7*) it is a very versatile NO_x reduction catalyst. In the present study, a reaction mechanism is postulated that is fairly analogous to the W mechanism (*3*) except that the reactive surface is not nitrided.

The decomposition of NH_3 has been studied on supported Rh (*5, 8*), Rh films (*6*), and polycrystalline Rh wire (*9*). The

[1] Present address: Monsanto Company-Q3B, 800 N. Lindbergh Blvd., St. Louis, Mo. 63166.

0021-9517/81/050158-14$02.00/0

results of these studies vary quite markedly as far as absolute reaction orders, activation energies, and relative reactivities are concerned. Only minimal interpretations of the results were given in all cases and no mechanisms proposed. The purpose of this investigation was to obtain results concerning the interaction of NH_3 with Rh which could be compared to the above-mentioned studies and to interpret these results in a self-consistent and chemically meaningful way. LEED/AES and flash desorption spectroscopy were used to characterize the catalyst surface under a variety of conditions. Reaction kinetics obtained from a static reactor with mass spectrometric product detection are correlated to a surface-specific reaction mechanism. An observed isotope effect very similar to that observed on W (*3*) is seen to be consistent with the proposed mechanism. Possible reasons for the marked face specificity observed in this and other studies (*3, 4*) are discussed.

EXPERIMENTAL

Introduction

The apparatus and procedures used were quite similar to those reported earlier (*3*). Only modifications will be mentioned here. Within the vacuum system, shown schematically in Fig. 1, the Rh single crystals could be degassed to 1500 K during cleaning cycles. A variable leak valve was used to continuously sample the reaction mixture into the mass spectrometer chamber. In most cases, the rate of N_2 production was monitored, via a mass spectrometer (EAI QUAD 150A) trace.

Sample Preparation

The Rh single-crystal samples were cut from a single-crystal ¼-in. rod from Materials Research Corporation. Back reflectance Laue X-ray patterns indicated that the (110), (100), and (111) samples cut were within ~1.0° of the desired orientations. The disk-like samples, following polishing, were ~7 × 0.6 mm. The samples contained a significant Pt impurity (few percent) which was evenly dispersed. The effect of this impurity was considered negligible as the surface concentration and reported relative NH_3 decomposition activity (*5*) of Pt were very small. Each crystal sample was spotwelded to a 0.25-mm Rh wire which was further welded to a 1-mm Rh rod. The edge area of a crystal was about 10% of the total area, so that edge reactivity may lead to overestimation of the reactivity of a relatively unreactive crystal face.

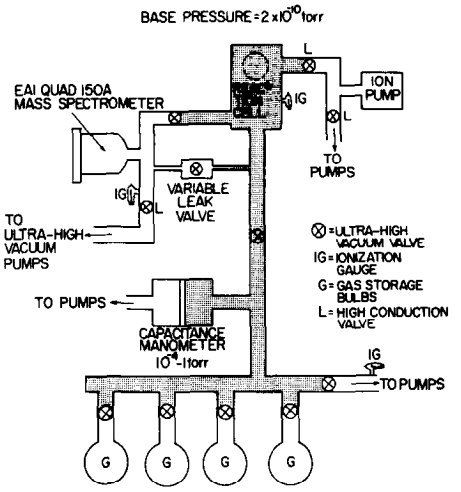

FIG. 1. Schematic of ultrahigh vacuum system used in kinetic and flash desorption experiments. (Shaded area = reaction volume ≅ 1.1 liters.)

Initially, the Rh (110) sample was argon-bombarded and heated in O_2 as recommended in the literature (*10–12*). The surface resulting from a single cleaning cycle showed very low, unstable catalytic activity, and a large number of cleaning cycles was required before the Rh (110) sample was stably active for the NH_3 decomposition reaction. Thereafter, flashing to 1400 K *in vacuo* adequately regenerated catalytic activity. As will be discussed later, it appears the presence of surface B caused the initial low activity. Once the B was depleted from the bulk, the activity stabilized. The Rh (100) and (111) surfaces were treated similarly before they were used in

the kinetic experiments. Auger and ESCA analysis of the Rh (110) and (100) faces indicated that the B concentration was very low following the above cleaning treatments; separate Auger experiments (see next section) showed that C, O, P, and S were easily removed by these same treatments.

Surface Characterization Procedures

An "untreated" Rh (110) sample was mounted on an offset Varian manipulator and installed in a Varian vacuum chamber equipped with the 4-grid LEED optics and Auger electron spectrometer with a CMA. (It should be noted that the LEED/AES system was distinct from that shown in Fig. 1, so that LEED/AES characterizations were performed in a system different from that used for kinetic and thermal desorption experiments.) Temperatures up to 1600 K were obtained using an indirect heater block. The AES experiments were run at 10 μA beam current, 2.0 keV beam energy, 100–1100 eV scan width (3.3 eV/sec), and 10 V peak-to-peak modulation. After initial outgassing, AES spectra indicated that the Rh surface was contaminated with P, S, and B. Extensive O_2 and Ar^+ treatments removed the P and S but the B persistently segregated to the surface. The B concentration was substantially reduced after several days of cleaning treatments.

Ammonia was dosed into the vacuum chamber via a leak valve. With the NH_3 pressure $\geq 10^{-7}$ Torr (1 Torr = $10^3 \mu$m = 133.3 N m^{-2}) the N (380-eV) peak was monitored as a function of sample temperature. The AES electron beam was on only when obtaining spectra as beam-induced NH_3 adsorption is possible (*13, 14*). To simulate kinetic reaction conditions, 70μm NH_3 were dosed into the isolated bell jar with the sample at ~650 K. Following pump down, the AES spectrum was taken to determine the N surface concentration.

Thermal desorption spectra were obtained with the Rh (110) sample used in the kinetic apparatus (Fig. 1). H_2 and NH_3 were adsorbed at pressures of about 10^{-8} Torr at 250 K and the sample temperature was raised at ~8 K/sec to 900 K using a focused radiant beam. The desorption peaks were recorded via mass spectrometer output and ion gauge current. The NH_3 desorption experiments were monitored by the mass spectrometer only as all the ion gauges were off during the experiments.

Kinetics Procedure

The gas-phase reaction mixtures consisted of pure NH_3, NH_3/H_2, and NH_3/N_2 combinations. Due to heating limitations, maximum usable pressures were 500, 150, and 250 μm for NH_3, H_2, and N_2, respectively. Ammonia orders were determined for pure NH_3 and NH_3/H_2 mixtures. The H_2 and N_2 reaction orders were determined using the appropriate mixtures.

During kinetic and flash desorption experiments, the sample temperature was maintained by radiant heat from a focused 1200-W projector bulb. The temperature was controlled by a solid-state device which monitored the thermocouple emf. The reaction rates determined were the same whether the NH_3 was admitted over a heated catalyst or dosed over a cool catalyst whose temperature was subsequently raised. For the isotope experiments, the NH_3 and ND_3 were dosed alternately, separated by extended pumping periods. Most of the kinetic data were obtained on the more active Rh (110) sample. The kinetic orders for the Rh (100) and (111) samples were the same as that for the (110). In all cases, the ratio of the rates of H_2 and N_2 production was within 15% of the stoichiometric 3 : 1 value. Focusing the lamp on any portion of the reaction vessel other than the crystal resulted in no reaction. When an initially cool crystal was illuminated reaction rates under our conditions were negligible until the crystal was hot (over 600 K) indicating negligible photochemical reaction.

The usable temperature range for the Rh (110) kinetic experiments was

$570 < T < 700$ K, limited at the low end by the limit of product detection and at the high end by the NH_3 conversion (>10%) over the reaction time period in the basically static reactor. Pressures had to be limited due to thermal conductivity heat losses and NH_3 decomposition in the mass spectrometer chamber.

The mass spectrometer signals for H_2 and N_2 were linear functions of the capacitance manometer pressures in the pressure range of interest. The effect of increasing background pressures in the reaction cell on the calibrations was accounted for in the final rate determinations.

Materials

The NH_3 (99.999%) was obtained from Scientific Gas Products in 1-liter bulbs and used without further purifications. The ND_3 was loaded from a Stohler Isotope Chemicals lecture bottle (~98%) into a 1-liter bulb and vacuum-distilled using 1-N_2 and dry ice–acetone slurries. Bulbs of N_2 (>99.999%) and H_2 (>99.999%) were purchased from Matheson Gas Products. Ar (99.999%) was obtained from the Linde Division of Union Carbide Corporation. O_2 was purified through a Ag diffuser.

RESULTS AND DISCUSSION

Surface Characterization

An "untreated" Rh (110) crystal was chosen for the LEED/AES experiments to investigate the initial "inactivity" of the Rh (110) used in the kinetic studies. The sample was subjected to a number of standard cleaning techniques. Figure 2 shows the Auger spectra taken following these treatments. Spectrum (a) was taken after only heating the crystal to 1400 K for several hours. In addition to the Rh peaks (200, 222, 256, and 302 eV), peaks at 118, 154, and 180 eV are attributed to P, S, and B, respectively. In general, C and O could be removed from the surface by heating to 1400 K. Several Ar^+ bombardments and high-temperature O_2 doses produced spectrum (b), showing the S is easily removed. Lengthy oxygen treatments with high-temperature flashes were required to remove the phosphorous and reduce the boron surface concentration. Figure 2c is the cleanest spectrum obtained, with a small amount of B still present. This spectrum compares favorably with other clean Rh spectra reported (*12, 15, 16*).

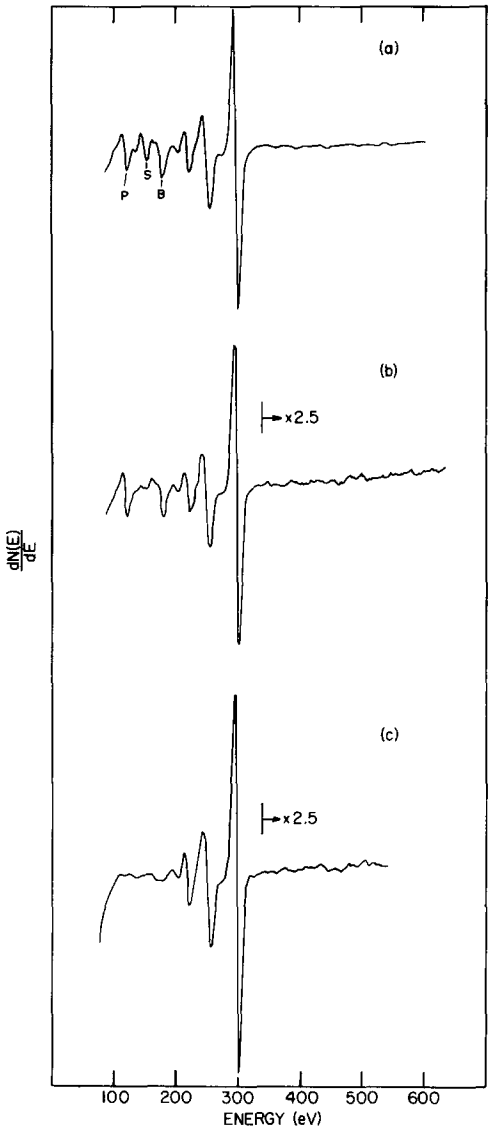

FIG. 2. Auger spectra of Rh (110) surface: (a) Initial spectrum after heating. (b) Spectrum after initial Ar^+ and O_2 treatment. (c) "Clean" Rh (110) spectrum.

Initially, NH_3 was absorbed at ~330 K

on the B-contaminated surface. As the temperature was raised, the N (380-eV) peak decreased slightly and then increased when $T > 770$ K. On cooling in a 10^{-7}-Torr NH_3 ambient, more B diffused out from the bulk. Figure 3a shows the resulting spectrum at 360 K, indicating a large amount of N (380 eV) and B (170–180 eV). The N peak would diminish only on heating to >1200 K, indicating the N was in the form of a boron nitride which has been observed on Rh (*17*). The presence of this surface nitride interfered with the detection of any nitrogen adsorbed on Rh alone. Extensive cleaning removed most of the B and made this interference negligible. Clearly, the initial low activity of the Rh (110) surface in kinetic experiments reflected the substantial boron contamination.

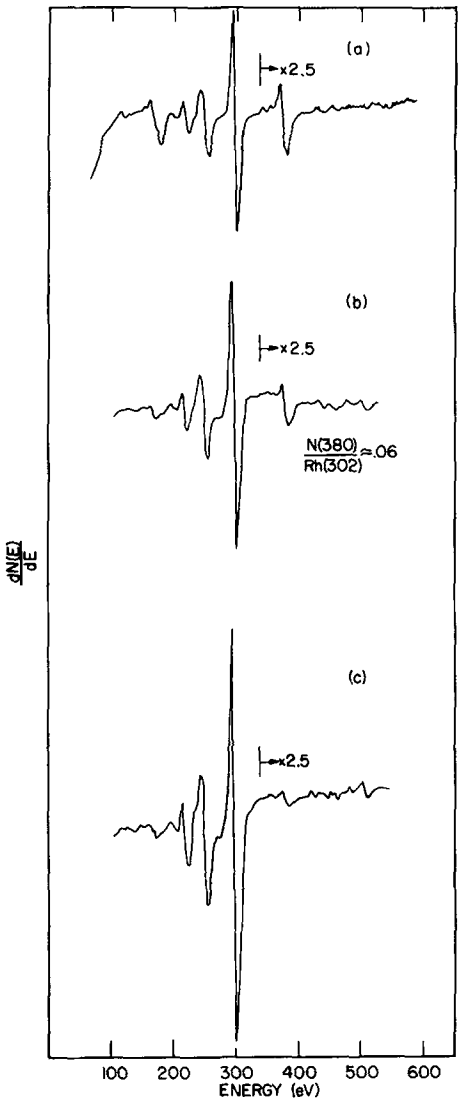

FIG. 3. Auger spectra obtained after NH_3 adsorption: (a) B-covered surface, indicating formation of surface boron nitride. (b) Saturated, "clean" surface with N peaks at 380 eV (T = 360 K). (c) Spectrum taken following 70-μm NH_3 dose at 650 K.

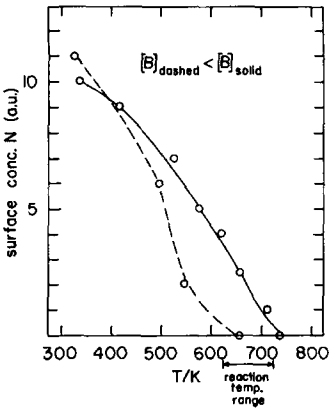

FIG. 4. Amount of adsorbed N as a function of catalyst temperature with $P_{NH_3} \approx 10^{-7}$–10^{-6} Torr throughout the experiment. (Dashed curve represents a more B free surface than the solid curve.)

Upon dosing 10^{-6} Torr NH_3 onto the "B-free" sample at 330 K for 2400 sec (Auger beam off), the spectrum in Fig. 3b was obtained, showing the presence of a nitrogen species. The N (380)/Rh (302) ratio is about 0.06; Danielson *et al.* (*18*) found 0.093 for the N (380)/Ru (273) ratio produced by NH_3 adsorption on Ru (0001), and by correlating this ratio with an apparent (2 × 2) LEED pattern, attributed it to a 0.50 monolayer. The temperature of the sample was progressively raised with spectra taken at various intervals. Figure 4 depicts the N (380) peak-to-peak height as a function of temperature. Clearly, under low-pressure conditions ($< 10^{-6}$ Torr NH_3), the concentration of surface nitrogen was quite small within the reaction temperature range. Following the high-pressure reaction experiment (70 μm NH_3, 660 K, 10 min), the spectrum shown in Fig. 3c was obtained,

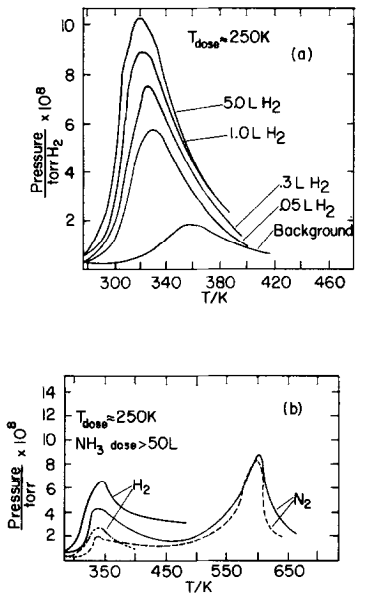

FIG. 5. Flash desorption spectra: (1 L = 10^{-6} Torr sec). (a) H_2 adsorption at 250 K. (b) NH_3 adsorption at 250 K (solid curves); NH_3 adsorption from ambient during cooling after initial flash (dashed curves).

indicating very little surface nitrogen present.

The adsorption of NH_3 on the Rh (110) surface produced no new diffraction spots on the (1 × 1) LEED pattern, but intensified the background causing the pattern to become quite diffuse. Similar behavior has been observed for NH_3 adsorption on Pt (*13*) and Ru (*14*) surfaces.

Flash desorption experiments involving H_2, NH_3, and N_2 interactions with the Rh (110) crystal were done in the reaction system (Fig. 1). Figure 5a shows the H_2 desorption curves obtained. The desorption temperature range of 320–360 K compares very favorably with the H_2 desorption range (300 to 370 K) from a Rh (111) surface observed by Yates and co-workers (*19*) and by Castner and Somorjai (*12*) from a stepped Rh surface. Clearly, there would be little adsorbed H on a Rh surface under vacuum conditions in the temperature range ($570 < T < 700$ K) of the kinetic studies.

Figure 5b shows the desorption results following NH_3 adsorption at 250 K. The H_2/N_2 peaks at ~350 K probably reflect decomposition of a surface species containing both nitrogen and hydrogen. In line with the reaction mechanism that will be discussed later, this species is presumed to be Rh_2NH. The dominating feature of the spectrum is the N_2 peak at 600 K which correlates quite well with the 650-K N_2 peak obtained by flash desorption of NO on Rh wire (*20*). No NH_3 desorption was observed; if any occurred the product NH_3 must have been largely adsorbed on the reaction vessel walls. Some N_2 and a CO peak at 540 K were observed following "activated" N_2 adsorption; the CO was probably from the background. The CO peak correlates well with the 530-K peak observed by Campbell and White (*21*).

The decrease in the low-temperature N_2, H_2 peaks for subsequent doses can be rationalized by the fact that the Rh (110) crystal was cooling in an ammonia ambient following a flash to 900 K, so that atomic N was deposited at $T < 600$ K. At the beginning of the flash (250 K), NH_3 adsorption was reduced because a substantial part of the surface was blocked by the atomic nitrogen.

The Auger and flash desorption results support the contention that the Rh surface

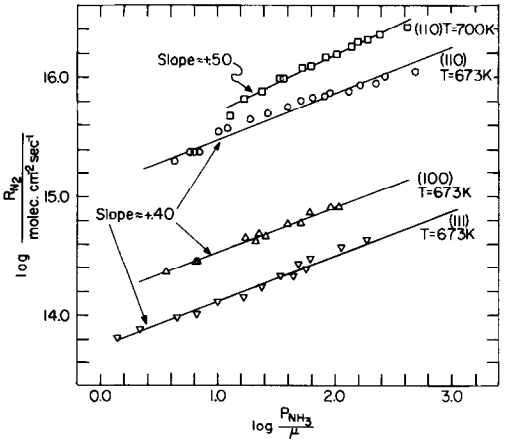

FIG. 6. The dependence of the reaction rate on ammonia pressure in pure NH_3 for the three crystals faces at 673 K. The face specificity is quite evident. (Top curve shows data at 700 K on the Rh (110).)

was nearly devoid of adatoms other than nitrogen at typical reaction temperatures for the NH_3 decomposition.

Kinetics Introduction

Table 1 summarizes the kinetic results obtained from the active Rh (110) single crystal. The results from the Rh (100) and (111) samples were similar with only a few reported.

Figure 6 shows the "pure" NH_3 kinetic order plots for the three crystal faces studied with $\sim\frac{1}{2}$ order in NH_3 indicated in all cases (the deviation toward first order at low P_{NH_3} and 700 K is believed to result from greater than 10% conversion in these experiments, so that sufficient hydrogen was produced to affect the reaction rate). The face specificity is quite evident, as is expected. As seen in Fig. 7, the rate of NH_3 decomposition is independent of N_2 over a wide pressure and temperature range, consistent with studies on numerous other metals (*2*). Figure 8 clearly shows the isotope effect observed on both the Rh (110) and (111) samples. The effect observed on Rh correlates well with that seen on W (*3*). Hence, the rate-limiting process should involve the breaking of a N–H bond.

The apparent activation energies of the NH_3 decomposition reaction can be extracted from Fig. 9. The values obtained are about 19 kcal/mole (1 kcal = 4.17 kJ) for all three faces. Similar equality of activation energies was found on Pt single crystals (*4*). The value of 19 kcal/mole correlates well with results on supported Rh (*5, 8*). With high H_2 pressures, the activation energy increased (Fig. 9b). The large value (57 kcal/mole) reported for Rh films (*6*) may be due to an extension of this trend, but even so it appears quite high.

During the complete analysis of the ki-

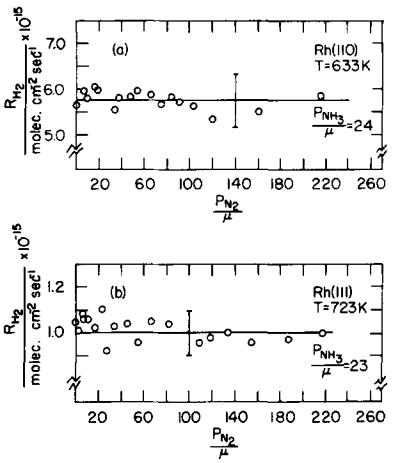

FIG. 7. Rate of H_2 production as a function of N_2 pressure: (a) Rh (110). (b) Rh (111). (Error bars are ~ ±10% of "average rate.")

TABLE 1

Summary of Kinetic Results on the Rh (110) Single Crystal

Conditions	Order
NH_3 orders[a]	
(1) Low P_{NH_3} ($P_{NH_3} < 30\mu$m), $P_{H_2} = 0$	$\sim +\frac{1}{2}$
(2) Moderate to high P_{NH_3} ($P_{NH_3} > 30\ \mu$m), $P_{H_2} = 0$	$\sim +\frac{1}{3}$
(3) Low P_{NH_3} ($P_{NH_3} < P_{H_2}$), P_{H_2} = constant $\neq 0$	$\sim +1$
(4) Moderate P_{NH_3} ($P_{NH_3} > P_{H_2}$), P_{H_2} = constant $\neq 0$	$\sim +\frac{1}{2}$
H_2 orders[b]	
(1) Low P_{H_2} ($P_{H_2} < P_{NH_3}$), P_{NH_3} = constant	0 → fractional (−)
(2) High P_{H_2} ($P_{H_2} > P_{NH_3}$), P_{NH_3} = constant	~ -1
N_2 orders	
(1) All temperatures and pressures	0

[a] Dependence on P_{H_2} and temperature is discussed in the text.
[b] Dependence on P_{NH_3} and temperature is discussed in the text.

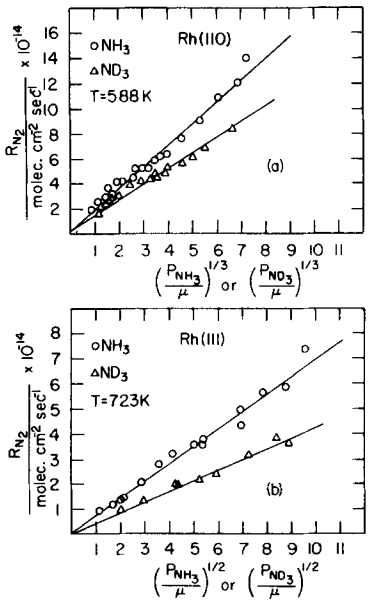

FIG. 8. Decomposition of NH_3 and ND_3 on (a) Rh (110); $r \cong 1.4$. (b) Rh (111); $r \approx 1.6$. r = rate (NH_3)/rate (ND_3).

netic data, it was noted that the rates varied by as much as 15% from day to day. These variations are assumed to be due to experimental errors; they were not due to sensitivity shifts as detector sensitivity was calibrated against the capacitance manometer during every set of experiments. To facilitate analysis, the following normalization procedure was used. Most of the data reported herein were taken at 633 and 673 K with a set of standard "pure" NH_3 runs performed after each experimental series. The rates determined from these runs were compared to a "standard" pure NH_3 order data set. All the data were then scaled such that the set of "pure" NH_3 runs correlated with the standard pure NH_3 order curve.

Mechanistic Considerations and Implications

The following mechanism for NH_3 decomposition on Rh is consistent with the observed reaction kinetic orders:

$$4Rh + NH_3(g) \underset{k_{-1}}{\overset{k_1}{\rightleftarrows}} Rh_2NH + 2RhH, \quad (1a)$$

$$Rh_2NH \xrightarrow{k_2} RhN + RhH, \quad (1b)$$

$$2RhH \underset{k_{-3}}{\overset{k_3}{\rightleftarrows}} 2Rh + H_2(g), \quad (1c)$$

$$2RhN \xrightarrow{k_4} 2Rh + N_2(g). \quad (1d)$$

In steady state, for a steady flow of nitrogen atoms through the reaction path and stoichiometry in the production of hydrogen we must have

$$k_1[Rh]^4 P_{NH_3} - k_{-1}[Rh_2NH]\,[RhH]^2 = k_2[Rh_2NH] = 2k_4[RhN]^2 = \tfrac{2}{3}\{k_3[RhH]^2 - k_{-3}[Rh]^2 P_{H_2}\}. \quad (2)$$

The rate of production of nitrogen molecules is then

$$R = k_4[RhN]^2 = \frac{k_2k_3 + k_{-1}k_{-3}P_{H_2}[Rh]^2}{6k_{-1}} \left[\left[1 + \frac{6k_2k_{-1}k_3k_1P_{NH_3}[Rh]^4}{(k_2k_3 + k_{-1}k_{-3}P_{H_2}[Rh]^2)^2}\right]^{1/2} - 1\right]. \quad (3)$$

If surface concentrations are expressed as coverage fractions, the flash desorption results suggest strongly that these fractions are very small compared to one under the reaction conditions studied for the hydrogen-containing species RhH and Rh_2NH. Let θ = [RhN]; then to a high degree of approximation [Rh] = $1 - \theta$. By substitut-

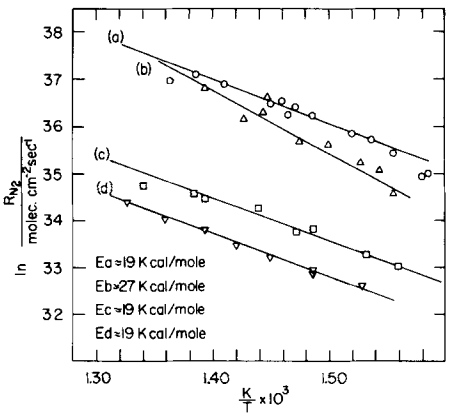

FIG. 9. Temperature dependence of decomposition rates: (a) Rh (110), P_{NH_3} = 29 μm. (b) Rh (110), P_{NH_3} = 29 μm, P_{H_2} = 31 μm. (c) Rh (110), P_{NH_3} = 24 μm. (d) Rh (111), P_{NH_3} = 29 μm.

ing these values in Eq. (3) and dividing by k_4, we obtain

$$\theta^2 = \frac{k_2k_3 + k_{-1}k_{-3}P_{H_2}(1-\theta)^2}{6k_4k_{-1}} \left[\left[1 + \frac{6k_1k_2k_3k_{-1}P_{NH_3}(1-\theta)^4}{\{k_2k_3 + k_{-1}k_{-3}P_{H_2}(1-\theta)^2\}^2}\right]^{1/2} - 1\right]. \quad (4)$$

Let $\alpha = k_2k_3/6k_4k_{-1}$, $\bar{P}_{H_2} = k_{-1}k_{-3}P_{H_2}/k_2k_3$, $\bar{P}_{NH_3} = 6k_1k_{-1}P_{NH_3}/k_2k_3$. Then Eq. (4) can be rearranged to

$$\theta^4 + 2\alpha\theta^2[1 + (1-\theta)^2\bar{P}_{H_2}] = \alpha^2(1-\theta)^4\bar{P}_{NH_3}. \quad (5)$$

In principle these equations can be solved for θ, and the rate of nitrogen production is then $k_4\theta^2$. The general solution is plainly awkward, but several limiting cases are readily explored.

(1) If $\theta^2 \ll 2\alpha[1 + (1-\theta)^2\bar{P}_{H_2}]$ the θ^4 term on the left side of Eq. (5) can be neglected and, approximately, $(1-\theta)^2\bar{P}_{H_2} = \bar{P}_{H_2}$, $(1-\theta)^4\bar{P}_{NH_3} = \bar{P}_{NH_3}$. Then

$$R = k_4\theta^2 = \tfrac{1}{2}k_4\alpha\bar{P}_{NH_3}/(1 + \bar{P}_{H_2}). \quad (6)$$

Two limiting subcases arise:

(*a*) If $\bar{P}_{H_2} \ll 1$

$$R = \tfrac{1}{2}k_4\alpha\bar{P}_{NH_3} = \tfrac{1}{2}k_1P_{NH_3}. \quad (7a)$$

The rate of decomposition is the rate of adsorption on a bare Rh surface; the reverse of steps (1a) and (1c) of the mechanism occur at negligible rates. Approximate surface compositions are implied by Eq. (2) with [Rh] = 1 neglecting terms with k_{-1} and k_{-3}. A rate first order in NH_3 was not observed in the absence of added hydrogen, implying that in the absence of added hydrogen θ was not negligible even at the lowest ammonia pressures investigated.

(*b*) If $\bar{P}_{H_2} \gg 1$

$$R = \tfrac{1}{2}k_4\alpha\bar{P}_{NH_3}/\bar{P}_{H_2} = \tfrac{1}{2}k_2\left(\frac{k_1}{k_{-1}}P_{NH_3}\right)\left(\frac{k_{-3}}{k_3}P_{NH_2}\right)^{-1}. \quad (7b)$$

This corresponds to the rate of decomposition of Rh_2NH in equilibrium with gaseous NH_3 and RhH, the latter being in equilibrium with gaseous H_2. The kinetic orders in ammonia and hydrogen implied by Eq. (7b) are indeed observed for $P_{H_2} \gg P_{NH_3}$, $0.1 < P_{NH_3} < 10$ μm.

(2) If $\theta^2 \gg 2\alpha[1 + (1-\theta)^2\bar{P}_{H_2}]$ the second term on the left side of Eq. (5) can be neglected. Then

$$R = k_4\{\alpha^{1/2}\bar{P}_{NH_3}^{1/4}/(1 + \alpha^{1/2}\bar{P}_{NH_3}^{1/4})\}^2. \quad (8)$$

This corresponds to the rate of decomposition of Rh_2NH in equilibrium with gaseous NH_3 and surface RhH on a surface partially blocked by nitrogen adatoms. Gaseous hydrogen is a negligible source of RhH, whose steady-state concentration is established by Eq. (2) with [Rh] = $1 - \theta$ and neglecting the term with k_{-3}. This is similar to the model used by McAllister and Hansen (*3*) to represent the decomposition of ammonia on tungsten. The kinetic orders in ammonia implied by Eq. (8), i.e., half-order in ammonia at low P_{NH_3}, decreasing at higher P_{NH_3}, and zero order in P_{H_2}, agree well with observations for $P_{NH_3} > P_{H_2}$, as indicated in Table 1.

A "bare surface limit" can be obtained by setting $(1-\theta) \approx 1$ in Eq. (4). Where $P_0 = (k_2k_3 + k_{-1}k_{-3}P_{H_2})^2/6k_1k_{-1}k_2k_3$ and $R_0 = (k_2k_3 + k_{-1}k_{-3}P_{H_2})/6k_{-1} = (k_1k_2k_3P_0/6k_{-1})^{1/2}$,

$$R/R_0 = [(1 + P_{NH_3}/P_0)^{1/2} - 1]. \quad (9)$$

For $P_{NH_3} \ll P_0$ use of the binomial expansion to leading terms leads immediately to Eq. (6) and so to its subcases Eqs. (7a) and (7b), while for $P_{NH_3} \gg P_0$ a similar expansion neglecting 1 compared to $(P_{NH_3}/P_0)^{1/2}$ leads to an approximation to Eq. (8) obtained by setting $(1 + \alpha^{1/2}P_{NH_3}^{1/4}) \approx 1$ in Eq. (8). A plot of log (R/R_0) vs log (P_{NH_3}/P_0) from Eq. (9) is a master plot on which plots of log R vs log P_{NH_3} at constant P_{H_2} should be superimposable under the "bare surface limit" model; the corresponding values of R_0 and P_0 can be obtained from the superposition. Figure 10 shows the best superposition of four data sets obtained at 673 K, and Fig. 11 shows the superposition of three data sets obtained at 633 K (see Table

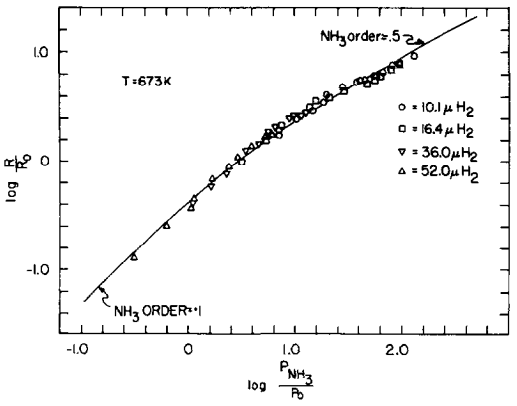

FIG. 10. Superposition of NH_3 order data at fixed P_{H_2} on log–log curve representing the function defined by Eq. (9) at 673 K (see Table 2 for appropriate parameters).

2 for parameters). The data shown are plainly rather well represented by Eq. (9). Further, from their definitions plots of $P_0^{1/2}$ vs P_{H_2} and R_0 vs P_{H_2} should be linear; Fig. 12 shows that such plots are in fact satisfactorily linear. Nevertheless, the "bare surface" model cannot account for ammonia kinetic orders less than one-half, and these are observed at higher ammonia pressures. Further, the slopes in Figs. 10 and 11 change very gently over the P_{NH_3}/P_0 range investigated; for $P_{NH_3}/P_0 < 1$, $R = \frac{1}{2}R_0P_{NH_3}/P_0$ (equivalent to Eq. (6)) differs from Eq. (9) by less than 21% so that resolution of R_0 and P_0 by superposition is somewhat ambiguous and the superposition can be chosen to improve linearity in plots such as those shown in Fig. 12. The ratio of slopes in plots of R_0 vs P_{H_2} and $P_0^{1/2}$ vs P_{H_2} should be equal to the ratio of intercepts; the ratios differ by about 30% in the plots shown. The slope in the plot of R_0 vs P_{H_2} is $k_{-3}/6$; the values for k_{-3} obtained from it, in 10^{14} molecules cm^{-2} sec^{-1} μm^{-1}, are 1.0 and 3.0 at 633 and 673 K with indicated activation energy about 24 kcal. In fact one would expect a very small activation energy for hydrogen adsorption on Rh, and a rate of adsorption close to the kinetic theory impact rate (i.e., $k_{-3} \approx 5 \times 10^{17}$ cm^{-2} sec^{-1} μm^{-1}). Hence the "bare surface" model, while leading to an equation which reasonably fits kinetic data in the presence of added hydrogen, does not lead to satisfactory parameter values when parameters are chosen to fit data for $P_{NH_3}/P_0 > 1$. It should be noted that a variant of this model can be obtained from Eq. (5) if the θ^4 term on the left side is neglected and if $(1-\theta)^2\tilde{P}_{H_2} \gg 1$. In this case we find

$$R = k_4(\tfrac{1}{2}\alpha\tilde{P}_{NH_3}/\tilde{P}_{H_2})\{1 + (\tfrac{1}{2}\alpha\tilde{P}_{NH_3}/\tilde{P}_{H_2})^{1/2}\}^{-2}. \quad (10)$$

This is equivalent to Eq. (9) for $\frac{1}{2}\alpha\tilde{P}_{NH_3}/\tilde{P}_{H_2} \ll 1$ and $k_{-1}k_{-3}P_{H_2} \gg k_2k_3$. It also, on substitution $R_0' = k_4$, $P_0' =$

TABLE 2

Parameters Obtained from Superposition of Data on log R/R_0, log P/P_0 Curve Defined by Eq. (5)

T (K)	P_{H_2} (μm)	R_0 (molecules cm^{-2} sec^{-1})	P_0 (μm)	$P_0^{1/2}$ ($\mu m^{1/2}$)	$R_0/P_0^{1/2}$ (molecules cm^{-2} sec^{-1} $\mu m^{-1/2}$)
673	10.1	8.1×10^{14}	1.00	1.00	8.10×10^{14}
	16.4	1.05×10^{15}	1.86	1.37	7.67×10^{14}
	36.0	2.04×10^{15}	7.94	2.82	7.24×10^{14}
	52.0	2.82×10^{15}	15.85	3.98	7.08×10^{14}
633	19.0	4.0×10^{14}	3.16	1.78	2.24×10^{14}
	26.5[a]	5.6×10^{14}	3.98	2.00	2.81×10^{14}
	37.5	6.9×10^{14}	10.00	3.16	2.19×10^{14}

[a] This data set was not included in subsequent slope and intercept determinations due to a large rate correction.

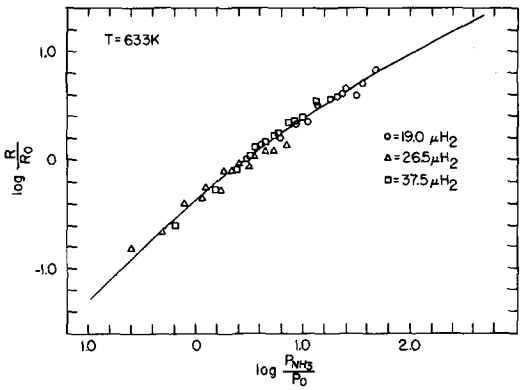

FIG. 11. Superposition of NH_3 order data at fixed P_{H_2} on log–log curve representing the function defined by Eq. (9) at 633 K (see Table 2 for parameters).

$2k_4k_{-1}k_{-3}P_{H_2}/k_1k_2k_3$, generates a master curve when $\log (R/R_0')$ is plotted against $\log (P_{NH_3}/P_0')$, which can be compared to that generated by Eq. (9). The two curves are essentially superimposable over the range $-1 \leq \log (P_{NH_3}/P_0) \leq 2$ covered in Fig. 11 on choices $P_0' \approx 56P_0$, $R_0' \approx 25R_0$ (for proper limiting correspondence as $(\frac{1}{2}\alpha\bar{P}_{NH_3}/\bar{P}_{H_2})^{1/2} \ll 1$ one should have exactly $R_0'/P_0' = \frac{1}{2}(R_0/P_0)$. Hence Eq. (10) can represent the data in Fig. 11 quite well; it provides one less adjustable parameter for interpreting the dependence of R_0' and P_0' on P_{H_2} and is hence somewhat less flexible than Eq. (9). It accounts for the reduction in P_{NH_3} kinetic order in quite a different and physically more satisfying manner than Eq. (9) as due to surface blockage by nitrogen adatoms (use of Eq. (10) for data in Fig. 11 indicates coverages in the range $0.07 < \theta < 0.5$). Values of about 10^{16} molecules cm^{-2} sec^{-1} for k_4 at 633 K and an activation energy of about 25 kcal for E_4 also seem reasonable values for nitrogen desorption.

In searching for a representation of the variation in rate with P_{H_2} at constant P_{NH_3} which is more convenient to use than Eq. (9), we found that this variation was rather well represented by

$$R_{0H}/R_H = 1 + kR_{0H}P_{H_2} \quad (P_{NH_3} \text{ constant}), \quad (11)$$

where R_H is the decomposition rate at P_{H_2}, and R_{0H} the decomposition rate at $P_{H_2} = 0$. This result is not at all suggested by Eqs. (9) or (10); a modified version of it has been used by Mardaleishvili *et al.* (*22*). Analysis of the dependence of k and R_{0H} on P_{NH_3} led to the following empirical rate law:

$$R_H = \frac{k''P_{NH_3}}{P_{NH_3}^n + k'''P_{H_2}}. \quad (12)$$

Noting that $R_{0H} = k''P_{NH_3}^{1-n}$, a plot of R_{0H}/R_H vs $P_{H_2}/P_{NH_3}^n$ should be linear; such plots are shown in Fig. 13. Best fits were obtained with $n = \frac{2}{3}$, $k'' = 5.1 \times 10^{14}$ molecules cm^{-2} sec^{-1} $\mu m^{-1/3}$, $k''' = 0.45$ $\mu m^{-1/3}$ at 633 K and $n = \frac{1}{2}$, $k'' = 1.04 \times 10^{15}$ molecules cm^{-2} sec^{-1} $\mu m^{-1/2}$, $k''' = 0.147$ $\mu m^{-1/2}$ at 673 K. These parameters were then used to calculate sets of points in the pressure range of interest (1 to 400 μm) which could be tested for superposition on the master curve generated by Eq. (9). Figure 14 shows that the superposition is quite good; in the pressure range tested the empirical equation (12) happens to have almost the same form as

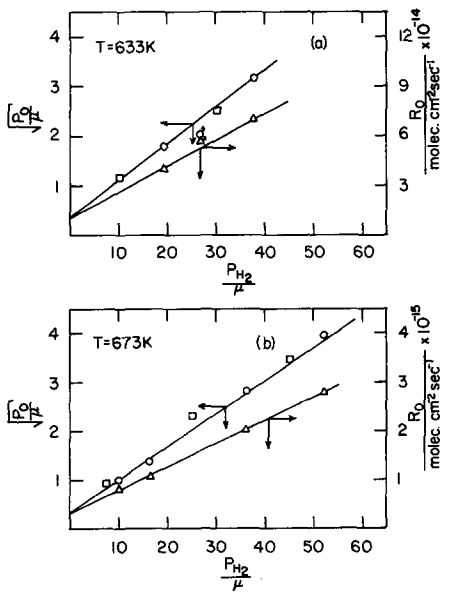

FIG. 12. Relation of $P_0^{1/2}$ (circles) and R_0 (triangles) to hydrogen pressure at (a) 633 K (see comments in text concerning starred points). (b) 673 K. (The squares are empirically determined as discussed in the text.)

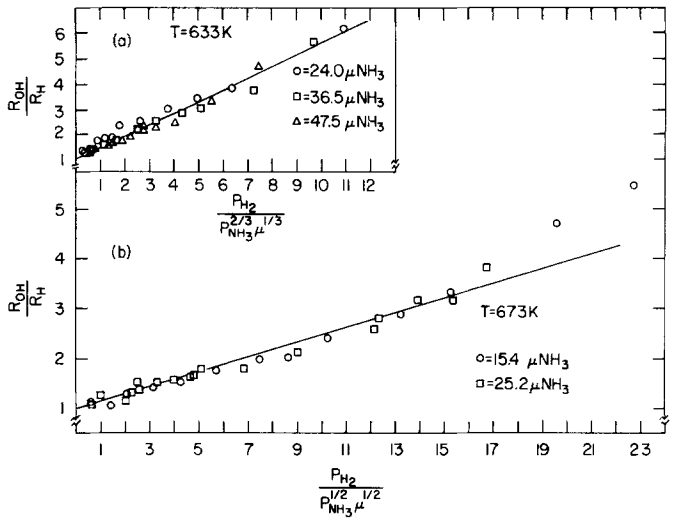

FIG. 13. Superposition of all H_2 order data on linear plots derived from $R_H = k''P_{NH_3}[P^n_{NH_3} + k'''P_{H_2}]^{-1}$.

Eq. (9). Values of P_0 and R_0 which can be obtained from the superposition, are shown as squares in Fig. 12, and plainly fit well with other points on the curves shown. The correspondence between Eqs. (9) and (12) must be limited in pressure range, e.g., at sufficiently high P_{NH_3} the rate must vary as $P^{1/2}_{NH_3}$ according to Eq. (9), as $P^{1-n}_{NH_3}$ according to Eq. (12).

Returning to the "higher-coverage" range covered by Eq. (8), let $\beta^2 = \alpha^2\bar{P}_{NH_3} = k_1k_2k_3P_{NH_3}/6k_4^2k_{-1}$. Then

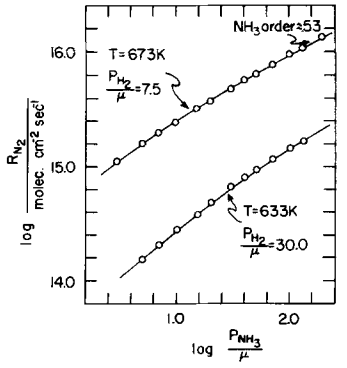

FIG. 14. Examples of the superposition of calculated data from Eq. (12) onto the mechanism "function." The values of $P_0^{1/2}$ obtained from these "empirical" superpositions are shown as squares in Fig. 12.

$$\theta = \beta^{1/2}[1 + \beta^{1/2}]^{-1}. \qquad (13)$$

Since $R = k_4\theta^2$ and $P_{NH_3} = P_1\beta^2$, where $P_1 = 6k_4^2k_{-1}/k_1k_2k_3$, a plot of log θ^2 vs log β^2 should furnish a master curve on which plots of log R vs log P_{NH_3} can be superimposed, with k_4, P_1, and the range of θ corresponding to the data obtainable from the superposition. Figure 15 shows that the data obtained in experiments at 633 K with no hydrogen added indeed satisfy this expectation; the correlation indicates a range $0.045 \leq \theta \leq 0.40$ for the data shown.

The range of kinetic orders and reaction rates (including their temperature dependence) are in general agreement with results reported by Sokol'skii *et al.* (*5*) and Amano and Taylor (*8*). A direct comparison with results of Pignet and Schmidt (*9*) is possible, as a rate of 8×10^{15} molecules cm^{-2} sec^{-1} at 115 μm and 673 K can be estimated for Rh wire by extrapolation of their Fig. 1. Our rate for Rh (110) under the same conditions was 7.5×10^{15} molecules cm^{-2} sec^{-1}. Rates found by Logan and Kemball (*6*) on evaporated films are lower by a factor of 10^3 than those found in the present work under comparable conditions, their activation energies are much higher,

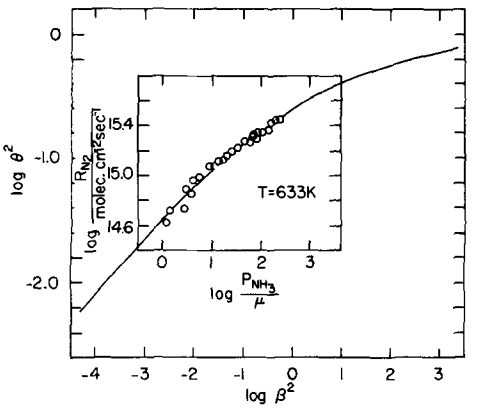

FIG. 15. Correlation of pure NH_3 data at 633 K with the log θ^2 *versus* log β^2 curve obtained from Eq. (13), showing the actual and theoretical decrease in NH_3 order. A value of 9×10^{15} molecules cm^{-2} sec^{-1} for k_4 is extracted from this curve and other available information.

and their reaction orders are quite different; their results appear generally at variance with the present work and other references cited.

Rhodium is an effective ammonia decomposition catalyst. Rates comparable to those obtained at 673 K on Rh require ~870 K on W (*3*). Comparison with a study on Pt single crystals (*4*) indicates that Rh is about 10 times as active as Pt, substantiating other contentions to this effect (*5, 6*).

The mechanism proposed generates the observed kinetics rather well but is doubtless not unique in this respect. The proposed intermediates are chemically reasonable; RhH presumably is a hydrogen atom σ bonded on top of a Rh atom but quite mobile at the temperatures under investigation, and Rh_2NH is an imino group bridged between two Rh atoms (the typical Rh–Rh distances of 0.269 and 0.380 nm on Rh (110) and Rh (100) can both accommodate such a group with reasonable bond angles although the lower distance would be more attractive and is also common on Rh (111)). A 4-coordination site has been claimed most attractive for nitrogen adsorption on tungsten (*23, 24*) and such sites are also available in the troughs on the Rh (110) surface and (in rather crowded form) on the Rh (100) face, but not on the (111) face; the RhN species is possibly of this character although the nitrogen adatoms would also be expected to be moderately mobile under reaction conditions. The order of increasing catalytic activity of crystal faces illustrated in Fig. 8 is also the order of decreasing density of surface metal atoms, the order of increasing numbers of missing neighbors for the surface metal atoms, and correspondingly of increasing numbers of orbitals in these surface metal atoms available for bonding to adsorbates. The catalytic activities of different crystal faces of tungsten for ammonia decomposition follow a similar pattern (*3*).

ACKNOWLEDGMENT

This work was supported by the U.S. Department of Energy, under Contract 7405-eng-82, Office of Basic Energy Sciences, Division of Materials Science.

REFERENCES

1. Klimisch, R. L., and Taylor, K. C., *Environ. Sci. Technol.* **1**, 127 (1973).
2. Bond, G. C., "Catalysis by Metals," Chap. 16. Academic Press, New York/London, 1962.
3. McAllister, J., and Hansen, R. S., *J. Chem. Phys.* **59**, 414 (1973).
4. Löffler, D. G., and Schmidt, L. D., *Surface Sci.* **59**, 195 (1976).
5. Sokol'skii, D. V., Kuzora, T. V., Kozin, L. F., and Shcherbak, A. I., *Dokl. Akad. Nauk SSSR* **230**, 620 (1976).
6. Logan, S. R., and Kemball, C., *Trans. Faraday Soc.* **56**, 144 (1960).
7. Schlatter, J. C., and Taylor, K. C., *J. Catal.* **49**, 42 (1977).
8. Amano, A., and Taylor, H., *J. Amer. Chem. Soc.* **76**, 4201 (1954).
9. Pignet, T., and Schmidt, L. D., *J. Catal.* **40**, 212 (1975).
10. Sexton, B. A., and Somorjai, G. A., *J. Catal.* **46**, 167 (1977).
11. Mitchell, K. A. R., Shepherd, F. R., Wilson, P. R., and Frost, D. C., *Surface Sci.* **64**, 737 (1977).
12. Castner, D. G., and Somorjai, G. A., *Surface Sci.* **83**, 60 (1979).
13. Gland, J. L., *Surface Sci.* **71**, 327 (1978).
14. Danielson, L. R., Dresser, M. J., Donaldson, E. E., and Sandstrom, D. R., *Surface Sci.* **71**, 615 (1978).

15. Grant, J. T., and Haas, T. W., *Surface Sci.* **21,** 76 (1970).
16. Marbrow, R. A., and Lambert, R. M., *Surface Sci.* **67,** 489 (1977).
17. Sexton, B. A., private communication.
18. Danielson, L. R., Dresser, M. J., Donaldson, E. E., and Sandstrom, D. R., *Surface Sci.* **71,** 599 (1978).
19. Yates, J. T., Jr., Thiel, P. A., and Weinberg, W. H., *Surface Sci.* **84,** 427 (1979).
20. Campbell, C. T., and White, J. M., *Appl. Surface Sci.* **1,** 347 (1978).
21. Campbell, C. T., and White, J. M., *J. Catal.* **54,** 289 (1978).
22. Mardaleishvili, R. E., Hu, H.-C., and Smorodinskaya, Zh. Yu., *Kinet. Katal.* **10,** 1278 (1969).
23. Adams, D. L., and Germer, L. H., *Surface Sci.* **26,** 109 (1971).
24. Anders, L. W., Hansen, R. S., and Bartell, L. S., *J. Chem. Phys.* **62,** 1641 (1975).